Transport and vortex pinning in micron-size superconducting Nb films

Lamya Ghenim, Jean-Yves Fortin, Gehui Wen, Xixiang Zhang, Claire Baraduc, Jean-Claude Villegier

HAL Id: hal-00002859

https://hal.archives-ouvertes.fr/hal-00002859

Submitted on 16 Sep 2004

Transport and vortex pinning in micron size superconducting Nb films

Lamya Ghenim*

Institut Laue-Langevin, B.P. 156, 38042 Grenoble, France and CNRS

Jean-Yves Fortin†

CNRS, Laboratoire de Physique Théorique, UMR7085,
3 rue de L'Université, 67084 Strasbourg Cedex, France

Wen Gehui, Xixiang Zhang

Department of Physics, HK University of Science and Technology, Clear Water Bay, Kowloon, Hong Kong

Claire Baraduc, Jean-Claude Villegier

Département de Recherche Fondamentale sur la Matière Condensée,
CEA-Grenoble, F-38054 Grenoble cedex 9, France.
(Dated: September 16, 2004)

We have carried out Hall measurements on thin films of Nb in the flux flow regime. The Hall bars were several microns in scale. Oscillations with magnetic field in the tranverse and longitudinal resistances between the depinning field B_d and the upper critical field B_{c2} are observed below T_c. The Hall effect may even change sign. The tranverse and longitudinal resistances are interpreted in terms of current-driven motion of vortices in in the presence of a few impurities. Simulations from time-dependent Ginzburg-Landau equations (TDGL) confirm this argument.

The conductivity in the flux-flow regime of type-II superconductors is determined by the dynamics of vortices. Since vortex motion in an applied external magnetic field is intrinsically at least two dimensional, to understand the transport the full conductivity tensor is needed [1, 2, 3]. In past studies of vortex matter [4], the current-voltage curves have been observed to have interesting effects such as aging and memory phenomena. Together with effects of hysteresis in the magnetization curves, these have been interpreted as the consequences of the motion of interacting vortices in a complex energy landscape with random potential. This provides a general explanation of memory effects, slow relaxation rates and sensitivity to initial conditions. In this paper we present experimental evidence of similar memory and pinning effects in Hall and resistance measurements of type-II thin films, using samples of micron dimension well below T_c. By relating these results to simulations of the dynamics of vortices interacting with one another and a vortex scattering potential, we will deduce a length scale for the vortex pinning potential.

Up to now, observed anomalies in the Hall effect close to T_c in bulk samples have been explained as being related to vortex motion damping [5] or plastic flow of the vortex lattice [6]. As we diminish the sample size, one would expect to reach a regime where the motion of a finite number of vortices must be considered. In order to simplify full vortex dynamics, in which one must consider motions of the vortex lines, we have fabricated planar samples with thickness $L_z = 800 - 1000$Å, comparable to the coherence length ξ at 4K. In this case the vortex core can be considered as a disk. We took a conventional superconductor, Nb, with samples as pure as possible to minimize pinning. Nb has the advantage that the bulk vortex structure has been studied in detail by neutron scattering [7] and microscopy [8]. The epitaxial samples (100) were grown by DC magnetron sputtering on R-plane sapphire at 600ºC and the eight-lead Hall bars processed by photolithography and reactive-ion etching (the bar area is $L_x \times L_y = 50\mu\text{m} \times 5\mu\text{m}$; the resistance probes, which are micron wide, are separated by $L_p = 10\mu\text{m}$). DC Hall resistance R_{xy} and magnetoresistance R_{xx} measurements were made in the flux-flow regime with current reversal in the B transverse configuration. To eliminate the effects of contact misalignment, the Hall resistance

*present address: DSV/DRDC Laboratoire Biopuces- Bât 4020, CEA-Grenoble, 17, rue des Martyrs, 38054 Grenoble, email:ghenim@dsvsud.cea.fr
†email:fortin@lpt1.u-strasbg.fr

was obtained by subtracting the positive and negative magnetic field data. The films had $T_c = 8.4K$ and a resistive ratio $\rho_{xx}(300K)/\rho_{xx}(10K) = 5.1$ with a carrier density $n_e \simeq 8.5 \times 10^{22} cm^{-3}$, obtained from the expression $R_{xy} = B/en_e L_z$ for the Hall resistance in the normal phase. The low resistance contacts on the Hall bars were made by Indium bonding. The measurements were made with a Quantum Design Magnetic Property Measurement System adapted for transport measurements, giving high stability as a function of magnetic field and temperature. Figure 1 shows magnetoresistance as a function of magnetic field at $T = 4K$, well below T_c at current $I = 200\mu A$. The resistance R_{xx} is zero for fields below B_d, the depinning field for vortices, and then increases to reach its normal state value at B_{c2}. From the upper critical field experimental value $B_{c2}(4K) \simeq 1.3T$, we use the Ginzburg-Landau theoretical expression $B_{c2}(T) = \phi_0/(2\pi\xi^2(T))$, where ϕ_0 is the flux quantum, to deduce approximatively the zero temperature coherence length $\xi_0 \simeq 115$ Å. From the carrier density n_e, the zero temperature London penetration length can be estimated using the expression $\lambda_0 = \sqrt{m_e/\mu_0 n_e e^2}$, which gives $\lambda_0 \simeq 180$ Å, where m_e is the electron mass, and we obtain $\kappa \simeq 1.6$. The electronic mean free path l_e is computed from the normal resistance R_{xx} at 4K using the Drude formula $l_e \simeq (1.264 \times 10^4 \Omega)n_e^{-2/3} L_p/(R_{xx}L_z L_y)$[9]. The value of the normal resistance at $4K$ is $R_{xx} \simeq 1.7\Omega$, based on Fig. 1 data, which gives $l_e \simeq 76$Å at this temperature, of the same order as the cohence length. The relatively large value of l_e for these thin films shows the good quality of the samples. The transverse resistance displays a more striking behaviour; it oscillates strongly between the depinning field B_d and B_{c2}. Above B_{c2} the Hall resistance recovers the behavior of the normal state: it is linear with field, with slope inversely proportional to the Nb carrier density. In the field range where R_{xy} oscillates, this resistance may even be negative. As seen in Fig. 2, in general a minimum of R_{xy} corresponds to a maximum of dR_{xx}/dB . If R_{xy} were dominated by a parasitic resistive component, this would tend to give maxima in R_{xy} where the oscillating part of R_{xx} is maximal, ie where dR_{xx}/dB is between extrema. Subtraction of positive and negative magnetic field Hall data was important to avoid such parasitic effects. We note that to observe the oscillations the magnetic field had to be swept very slowly: typically at least 12 hours per scan for a given temperature.
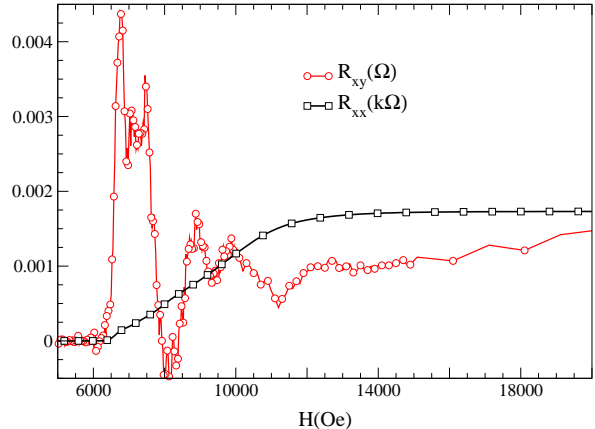

FIG. 1: Resistances for a sample size $L_p \times L_y = 10\mu m \times 5\mu m$, T=4K, I=200$\mu$A. For convenience R_{xx} is scaled by a factor 10^{-3}.
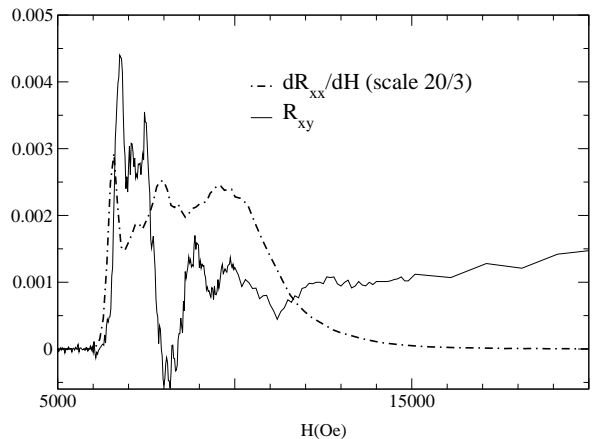

FIG. 2: Comparison of R_{xy} and dR_{xx}/dH. The parameters are the same as for Figure 1.

Figure 3 shows R_{xy} versus B for 2 different temperatures. As we heat the sample (from 4K) the oscillations in R_{xy} diminish as T approaches T_c over the narrowing field range between the depinning and the upper critical fields. Measurements at different longitudinal currents are shown in Fig. 4, from which we conclude that the oscillations are a low current phenomena: at $800\mu A$ they have almost disappeared. At low currents, the sign may be inverted (compare the data for 100 and $200\mu A$). In fact we observe inverted curves in different field scans at the same current (see insert of Fig. 4). Between these
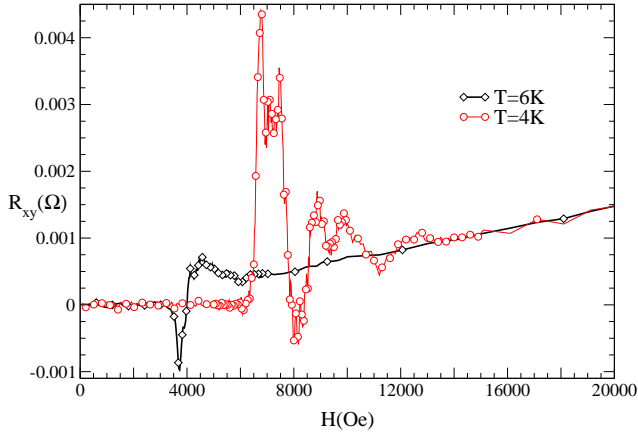
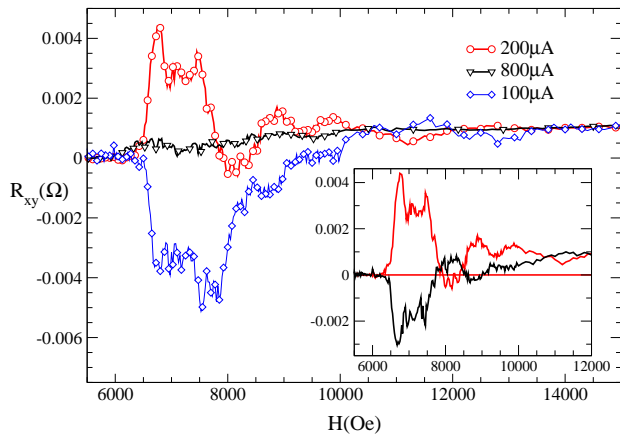FIG. 3: Transverse resistance for different temperatures, I=200μA.

FIG. 4: Transverse resistance for different currents, T=4K. In insert, different scans for the same current 200μA, showing history dependence.

scans the sample is kept at low temperature but was subject to different currents and fields. What is surprising is that while the oscillating part of the Hall conductivity is inverted, the pattern is very similar. The sign inversion invites comparison to the anomalous sign change observed in the Hall resistance near T_c in the bulk [5], described phenomenologically in terms of a vortex velocity which has a component opposite to the direction of the superfluid flow. Zhu et al. [6] related the sign reversal of the mixed-state Hall resistivity close to the critical temperature to thermal fluctuations and vortex-vortex

interactions and associated this inversion of sign to incoherent motion of vortices, i.e. plastic flow of vortex lattice. Here the sign reversal is of an oscillating transverse Hall effect and is most visible at low temperatures rather than as a smooth change of sign close to T_c, but we retain from the comparison that it must be related to the dynamics of interacting vortices. *Periodic* sharp oscillations in the resistance have been observed in superconducting Nb films with a square lattice of artificial pinning centers and are associated with commensurability of the vortex and antidots densities [10, 11]. Thus the oscillations could be due to pinning. The inversions we see indicate that for a fixed configuration of defects the overall sign depends on the initial vortex configuration. The two striking features of our results: sharp oscillations and sensitivity to initial conditions, lead us to propose a dynamical model including both vortex interaction and a quenched pinning potential. In order to describe the evolution in time of the local superconducting and normal flows, and local induced magnetic field, we use the TDGL equations [12, 13, 14, 15, 16, 17]. They are time- and space- dependent nonlinear differential equations coupling the superconducting order parameter and the vector potential and are useful to predict qualitative effects of vortex dynamics in the mixed phase of type-II material. The TDGL equations are derived from the extremum of the superconductor free energy in presence of an external magnetic field $\mathbf{B}_e$ perpendicular to the sample:

$$\mathcal{F} = \frac{a}{2}|\psi|^2 + \frac{b}{4}|\psi|^4 + \frac{1}{2m_s}\left|\left(\frac{\hbar}{i}\nabla - q_s\mathbf{A}\right)\psi\right|^2$$
$$+ \frac{1}{2\mu_0}\mathbf{B}^2 - \frac{1}{\mu_0}\mathbf{B}_e.\mathbf{B} \tag{1}$$

$\psi(\mathbf{r}, t)$ is the order parameter of the superconducting phase and we choose a gauge where the scalar potential is zero. The coefficient a is proportional to $(T - T_c)$ and is negative in the superconducting region. b does not depend on the temperature and is positive. $m_s = 2m_e$ and $q_s = 2q_e$ are the mass and charge of the Cooper pair. The steady state solution in the mixed phase in the absence of current is an Abrikosov vortex array. The interactions between vortices are included inside the non linear terms of the differential equations. Inside the vortex cores the magnetic field is maximum and superconducting density minimum. When a homogeneous current $\mathbf{J}$ is applied to one direction the vortex array moves in the trans-

verse direction in the absence of pinning. The current is introduced as a boundary condition. It is the sum of the contribution from the normal and superfluid components: $\mathbf{J} = \hat{\sigma}\mathbf{E} + \mathbf{J}_s$, $\mathbf{J}_s = q_s/m_s \Re\left[\bar{\psi}\left(-i\hbar\nabla - q_s\mathbf{A}\right)\psi\right]$. The conductivity tensor $\hat{\sigma}$ is the inverse of the classical resistivity tensor $\hat{\rho}$. The uniform equilibrium value of ψ [Eq. (1)] in the absence of a magnetic field can be simply written as $\psi_0 = \sqrt{-a/b}$, with $a = -a'(1 - T/T_c)$, a' is a positive constant. a' and b are related to the zero temperature coherence and penetration lengths by $\xi_0 = \hbar/\sqrt{2m_s a'}$ and $\lambda_0^2 = m_s b/(\mu_0 q_s^2 a')$. Within the domain of applicability of the TDGL theory, all material parameters can be reduced to the following units:

$$
\begin{aligned}
\text{lengths } L &\rightarrow L/\xi_0, \qquad (2)\\
\text{temperature } T &\rightarrow T/T_c,\\
\text{magnetic field } B &\rightarrow B/B_{c2}(0),\\
\text{potential vector } \mathbf{A} &\rightarrow \mathbf{A}/B_{c2}(0)\xi_0\\
\text{wavefunction } \psi &\rightarrow \psi/\psi_0
\end{aligned}
$$

This allows one to study numerically general features of Nb films with only a few dimensionless parameters like κ or reduced temperature $t = T/T_c$. The time τ is defined in units of $\tau_0 = \mu_0\kappa^2\xi_0^2\sigma_n n_n(T)/n_e$, where n_n is the normal electron density, and σ_n the normal regime conductivity. The dimensionless equation of motion for ψ reads:

$$
\frac{\partial\psi}{\partial\tau} = \frac{1}{\eta}\left[-\left(\frac{1}{i}\nabla - \mathbf{A}\right)^2\psi + (1-t)\left(1 - |\psi|^2\right)\psi\right], \quad (3)
$$

where η is a relaxation rate proportional to the product of a dimensionless constant $m_e/(\kappa^2\hbar\mu_0\sigma_n)$ and a numerical value. This numerical value can be estimated from the Bardeen-Cooper-Schrieffer theory[18, 19]. Taking the experimental values (see Table 1), the dimensionless constant is close to 20. In references[15, 19, 20], η varies from 0.8 to 12, and we will choose its numerical value around unity to optimize time convergence. From the Maxwell equations we obtain:

$$
\begin{aligned}
\frac{\partial\mathbf{A}}{\partial\tau} = \hat{\rho}&\left(-\kappa^2\nabla\times(\nabla\times\mathbf{A})\right.\\
&\left.+(1-t)\Re\left[\bar{\psi}\left(\frac{1}{i}\nabla - \mathbf{A}\right)\psi\right]\right), \quad (4)
\end{aligned}
$$

where $\rho_{x,x} = \rho_{y,y} = 1$ and $\rho_{y,x} = -\rho_{x,y} = \alpha B$ are the normal state components of the resistivity tensor in di-

mensionless units. The coefficient $\alpha = \sigma_n B_{c2}/q_e n_e$ is small ($\alpha \simeq 10^{-3}$ with the values of Table 1). In the following, we choose $\kappa = 2$ (to be clearly type II and close to the experimental value) and T= 0. Equations 3 and 4 are discretized on a grid of size $N\xi_0 \times N\xi_0$ with time step $\Delta\tau = 0.04$. It ensures that the equations converge to a unique steady solution. Taking different time steps around this value does not change the numerical results. Instead of using a discretized version of the vector potential $\mathbf{A}_{i,j}(\tau)$, we consider the link variables $U_{i,j}^\mu(\tau) = \exp(-iA_{\mu,i,j}(\tau)\,a_\mu)$, $\mu = x, y$, which preserve the gauge invariance properties of the continuous model [16, 21]. The resulting equations are accurate to second order in space and time steps. From the time dependence of the link variables, we obtain the instantaneous electric fields and the time averaged resistances.

We calculate with an external field B_e perpendicular to the sample and a bulk current $\mathbf{J}$ along the x axis, in units of $J_0 = q_e\hbar n_s(T)/(2m_e\xi_0)$, with $n_s(T) = n_e - n_n(T)$ the superconducting electron density. At zero temperature, given the experimental values (Table 1), this gives a current density $J_0 \simeq 6.85 \times 10^{13}\,\mathrm{A\,m^{-2}}$. The wavefunction and magnetic field are periodic along the x axis and ψ vanishes on boundaries of the transverse direction, where the magnetic field takes the values $B_e \pm \Delta B$, $\Delta B = JL_y/2\kappa^2$ being the contribution from the current introduced here as a boundary condition. At the beginning of the numerical simulation ($t = 0$ and $B_e = 0$), we take as initial conditions $\psi = 1$ in the bulk of the sample and small random values around zero for the potential vector components A_x and A_y. After an equilibration time, a few thousand time steps N_0, we switch on the current and measure the resistances, over a period of time $\tau = N_t\tau_0$ for each value of the external field B_e, where N_0 and N_t are the number of iterations of the equations. Every time we increase the external magnetic field by a small amount, we let the system approach the steady state during N_0 time steps before recording the resistance values.

We model the "defects" in the sample (grain boundaries, thickness variations, the specific geometry....) by considering a square lattice of points where *either* the wavefunction vanishes $\psi \sim 0$, *or* it is fixed to a non-zero value depending on the superfluid density $\psi \sim |1 - B/B_{c2}|$. In the first case the impurities decrease the local condensate density and attract vortices while in the second case they repel. Because the pinning potential is

periodic, it is characterised by a distance between centers denoted by L_{imp}. L_{imp} is the distance between vortex scattering centers, to be distinguished from l_e which is the distance between elastic scattering centers for electrons. For simplicity, we choosed a periodic structure for the impurities instead of a random one. This is in order to study the influence of the impurity density, considered as a single parameter, on the voltage oscillations. In the simulations L_{imp} varies from 3.33 (36 impurities, $N = 20$) to 12.5 (1 impurity, $N = 25$). In Fig. 5 we show the simulations for two different impurity concentrations together with the zero impurity case, shown to indicate the noise in the calculations. The oscillations in the transverse resistance, which are similar for the two forms of pinning potential, strongly resemble those seen in the experiments. From the numerical data, and from the range of system size studied (N=20-25 coherent lengths), we can extract a characteristic period δB, or equivalently a length $L_c \equiv 1/\sqrt{\delta B}$, and plot it as a function of L_{imp}, as shown in the insert of Fig. 5. It is seen to decrease with increasing L_{imp}, i.e. δB increases with increasing purity. From the dominant period of the experimental oscillations (Fig. 1) we can extract from the insert of Fig. 5 an effective distance for vortex pinning $L_{imp} \simeq 15 - 20\xi_0 = 0.17 - 0.23\mu m$. We use $\xi_0 = 115\text{Å}$ and assume we can apply the numerically derived relation between L_{imp} and L_c to our experimental sample. Indeed, the curve $L_c(L_{imp})$ depends on the parameters of the equations 3 and 4, in particular κ, the temperature and the ratio between the system size and the coherent length. Strictly speaking, the TDGL theory may not be accurate in the field range where we extracted L_c, but we expect to obtain a reasonable estimate of L_c for κ around the experimental value 1.6.

In Fig. 6 we calculate R_{xy} for two different currents: just as in the experiment (Fig. 4) if the current increases, the oscillation amplitude decreases. Furthermore we observe sign inversion due to differing initial conditions as shown in Fig. 7. The simulations then reproduce the experimental observation of a strong memory effect: while there is correlation in the positions of extrema, the nature of each extremum (maximum or minimum) depends on the initial condition at B_d, but is conserved through the scan. These simulations, which do *not* have the geometric features of the contacts, show that the effects seen experimentally are properties of *generic small* devices, and are not just an effect of the specific Hall bar geometry. It is
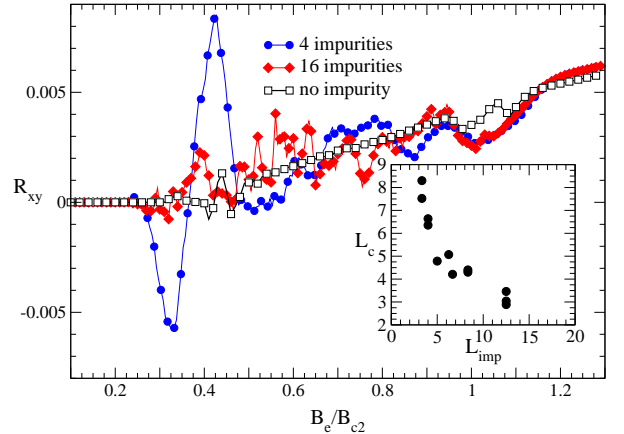

FIG. 5: Calculated transverse resistances for different impurity densities. In insert is L_c versus L_{imp} in units of the coherence length ξ_0. Parameters, whose definitions are in the text, are $N = 25$, $J = 0.03$, $N_t = 50000$, and $\eta = 0.5$.
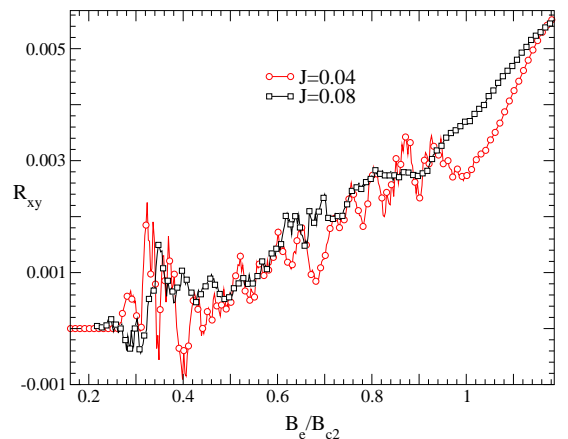

FIG. 6: Calculated transverse resistances for 2 different currents. Parameters are: $N = 20$, 9 impurities, $N_t = 50000$, and $\eta = 0.8$.

not excluded, however, that the boundaries of the device contribute to the pinning potential.

In conclusion, we have shown that micron scale Hall bars of thin films display strong oscillations in the transport in the flux-flow regime, in particular in the Hall voltage at low current. We have shown numerically that these oscillations may be explained by the effects of pinning potentials. The transverse voltage is proportional to the average vortex velocity in the longitudinal direction, which is much smaller than the velocity transverse to the
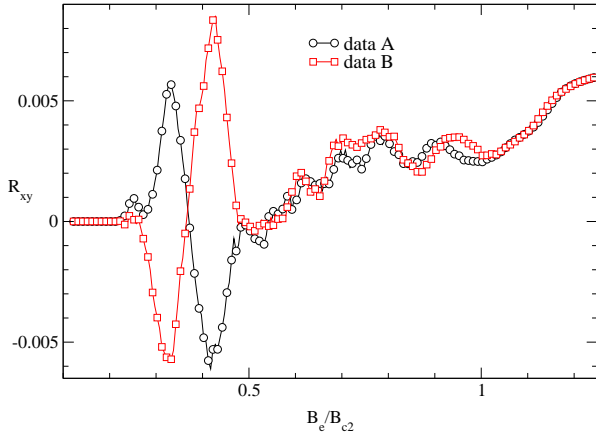
FIG. 7: Sign inversion seen for different random initial conditions A and B. Parameters are: $N = 20$, 4 impurities, $J = 0.03$, $N_t = 50000$, and $\eta = 0.8$.

current ($R_{xy}/R_{xx} \simeq 10^{-3}$). R_{xy} is therefore sensitive to the presence of bulk impurities which act as scattering centers for the vortices. As the transverse component of the vortex velocity is much larger than the longitudinal component, a small change in the velocity will have a much larger *relative* effect on its longitudinal component, hence R_{xy}. We explain the sign inversion seen experimentally (Fig. 4) and numerically (Fig. 7) by the fact that each vortex can be scattered by an impurity in two opposite directions, depending on its initial coordinates. The effect is amplified by the collective behavior of other vortices which tend to follow the same direction due to the stiffness of the vortex array. The surprising memory effect, that the inversion continues for the whole field scan, is reproduced by our model of quenched impurities, at least for the lower field range $B/B_{c2} \lesssim 0.6$. The abnormal Hall effect here is due to pinning of correlated vortices [22] and not to the dynamics of a single vortex. Thus even potentials of short range, as used in the simulations, are sufficient to influence the transport. Low current transport measurements are then a useful probe of vortex pinning potentials. These potentials are responsible for the complex behavior, as seen here and in other studies of bulk samples [4] that also showed aging and memory phenomena in the current-voltage caracteristics for example. From the experimental oscillations (Fig. 1) and assuming the caracteristic curve L_c versus L_{imp} is accurate for the samples studied, we extracted an effective distance $L_{imp} \simeq 0.17 - 0.23\mu$m between pinning

centers, for $\xi_0 = 115$Å, coherent with the large amplitudes seen. Our device is small enough and clean enough that there are a small number of effective pinning centers. More generally we can argue that in micron and, by extension, submicron superconducting devices, strong oscillations in the transport are to be expected as generic properties.

Table 1

Parameters	Experimental Values
$L_x \times L_y \times L_z$	50μm$\times 5\mu$m$\times 1000$Å
T_c	8.4K
n_e	8.5×10^{22}cm^{-3}
λ_0	180Å
ξ_0	115Å
κ	1.6
B_{c2}	1.3T (4K)
R_{xx} (normal state)	1.7Ω (4K)
σ_n (normal state)	$1.2 \times 10^7 \Omega^{-1}$m^{-1} (4K)
l_e	76Å(4K)

[1] S. J. Hagen et al., Phys. Rev. B **47**, 1064 (1993).
[2] J. Bardeen and M. J. Stephen, Phys. Rev. **140**, A1197 (1965).
[3] P. Nozières and W. F. Vinen, Philos. Mag. **14**, 667 (1966).
[4] M. Nicodemi and H.J. Jensen, J. Phys. A **34**, 8425 (2001). This reviews both experimental and numerical studies of aging and memory effects in vortex matter.
[5] S. J. Hagen et al., Phys. Rev. B **41**, R11630 (1990).
[6] B.Y. Zhu et al., Phys. Rev. B **60**, 3080 (1999).
[7] X. S. Ling et al., Phys. Rev. Lett. **86**, 712 (2001).
[8] C. Sow et al., Phys. Rev. Lett. **80**, 2693 (1998).
[9] N.W. Ashcroft and N.D. Mermin, *Solid State Physics*, Saunders College Publishing, New York, 1976, p757.
[10] V. Metlushko et al, Phys. Rev. B **60**, R12 585 (1999).
[11] C. Reichhardt, C.J. Olson, and Franco Nori, Phys. Rev. B **57**, 7937 (1998).
[12] C.-R. Hu and R.S. Thompson, Phys. Rev. B **6**, 110 (1972).
[13] M.M. Doria, J.E. Gubernatis, and D. Rainer, Phys. Rev. B **41**, 6335 (1990).
[14] Y. Enomoto and R. Kato, J. Phys.:Condens. Matter **3**, 375 (1991).
[15] R. Kato, Y. Enomoto, and S. Maekawa, Phys. Rev. B **44**, 6916 (1991).
[16] R. Kato, Y. Enomoto, and S. Maekawa, Phys. Rev. B **47**, 8016 (1993).
[17] C. Bolech, G.C. Buscaglia, and A. López, Phys. Rev. B **52**, R15 719 (1995).

[18] M. Tinkham, *Introduction to Superconductivity*, Edited by McGraw-Hill International (Singapore, 1996).

[19] A.D. Hernandez and D. Dominguez, Phys. Rev. B **65**, 144529 (2002).

[20] F. Liu, M. Mondello, and N. Goldenfeld, Phys. Rev. Lett. **66**, 3071 (1991).

[21] J.B. Kogut, Rev. Mod. Phys. **51**, 659 (1979). See page 690 for gauge invariance preservation of the GL equations by the introduction of link variables.

[22] P. Ao, J. Phys.: Condens. Matter **10**, L677 (1998).